

# Quantum phenomena in a chirped parametric anharmonic oscillator

I. Barth and L. Friedland

Racah Institute of Physics, Hebrew University of Jerusalem, Jerusalem 91904, Israel

The parametric ladder climbing (successive Landau-Zener-type transitions) and the quantum saturation of the threshold for the classical parametric autoresonance due to the zero point fluctuations at low temperatures are discussed. The probability for capture into the chirped parametric resonance is found by solving the Schrodinger equation in the energy basis and the associated resonant phase space dynamics is illustrated via the Wigner distribution. The numerical threshold for the efficient capture into the resonance is compared with the classical and quantum theories in different parameter regimes.

PACS numbers: 03.65.-w, 42.50.Lc, 05.45.Xt, 85.25.Cp

*Introduction.-* The parametric resonance is one of the most interesting and frequently used phenomena in classical and quantum dynamics. It occurs when the natural frequency of a system depends on a parameter oscillating (modulated) at twice the natural system's frequency [1–5]. In the well studied stationary case, the modulation frequency is constant. However, in nonlinear systems the stationary parametric amplification is restricted to small amplitudes, since at larger amplitudes the resonance (phase-locking) is destroyed due to the nonlinear frequency shift [1]. A robust method to overcome this limitation is to slowly vary the modulation frequency so that the resonance condition is preserved despite the increase of the amplitude of oscillations. This nonstationary phenomenon is called *parametric autoresonance* (PAR). The PAR was studied in such classical oscillatory systems as the anharmonic oscillator [6, 7], Faraday waves [8, 9], and plasmas [10]. A related, but different control method is the direct autoresonance (AR), where instead of parametric modulations, a chirped *external* driving force is applied. The direct AR was extensively studied and implemented in various classical and quantum physical systems [10–15].

When studying the classical to quantum transitions in the direct chirped-driven oscillator, one identifies two limits, where quantum dynamical effects are significant. The first is the saturation of temperature-dependent classical observables at small temperatures due to the zero point quantum fluctuations [16, 17]. In the second limit, at sufficiently large anharmonicity, the smooth classical AR dynamics of many simultaneously coupled energy levels transforms into a quantum ladder climbing involving successive two-level Landau-Zener (LZ) transitions [17–20]. These two quantum limits were also studied recently in the case of the direct chirped subharmonic (two-photon) resonance [21]. This letter, for the first time, discusses the analogous quantum phenomena in application to the PAR.

*The model.-* The simplest system exhibiting nonlinear parametric resonance is the anharmonic oscillator governed by Hamiltonian

$$H = \frac{p^2}{2} + (1 + \varepsilon \cos \varphi) \frac{x^2}{2} + \beta \frac{x^4}{4} \quad (1)$$

(here and below all variables and parameters are dimensionless). The frequency of the modulation is chirped,  $\omega \equiv d\varphi/dt = 2 + \alpha t$ , passing the linear resonance at  $t = 0$ . We expand the wave function of the oscillator,  $|\psi\rangle = \sum_n c_n |\psi_n\rangle$ , in the energy basis  $|\psi_n\rangle$  of the unmodulated Hamiltonian i.e.,  $H(\varepsilon = 0)|\psi_n\rangle = E_n|\psi_n\rangle$  and  $\langle\psi_k|\psi_n\rangle = \delta_{k,n}$ . In this basis, the dimensionless ( $\hbar = 1$ ) Schrodinger equation is

$$i \frac{dc_n}{dt} = E_n c_n + \frac{\varepsilon}{2} \sum_k c_k \langle\psi_k|\hat{x}^2|\psi_n\rangle \cos \varphi, \quad (2)$$

where for small  $\beta$ , the energy levels can be approximated as [22]

$$E_n \approx n + \frac{1}{2} + \gamma(n^2 + n) + \frac{3}{16}\beta, \quad (3)$$

$n = 0, 1, 2, \dots$ , and  $\gamma = \frac{3}{8}\beta$ . We also assume weak coupling,  $\varepsilon \ll 1$ , and, consequently, neglect the nonlinear corrections of order  $\beta$  in the coupling term,  $\langle\psi_k|\hat{x}^2|\psi_n\rangle \approx \frac{1}{2}[\sqrt{Q_n}\delta_{k,n-2} + (2n+1)\delta_{k,n} + \sqrt{Q_{n+1}}\delta_{k,n+2}]$ , where  $Q_n = n(n+1)$ . The resulting equation for  $c_n$  is

$$i \frac{dc_n}{dt} = E_n c_n + \frac{\varepsilon}{4}(\sqrt{Q_{n-1}}c_{n-2} + (2n+1)c_n + \sqrt{Q_{n+1}}c_{n+2}) \cos \varphi. \quad (4)$$

*Numerical examples.-* At this stage, we illustrate the PLC and the PAR in simulations. We have solved Eq. (4) numerically, subject to ground state initial conditions,  $c_n(t_0 = -10/\sqrt{\alpha}) = \delta_{n,0}$ , for two sets of parameters representing the quantum PLC (see Fig. 1(a,c)) and the classical PAR (Fig. 1(b,d)). In the first example,  $\{\alpha, \beta, \varepsilon\} = \{10^{-6}, 0.01, 0.04\}$  and 40 energy levels are included in simulations. The energy of the system versus the slow time  $\tau = \sqrt{\alpha}t$  is shown in Fig. 1(a). One can see that the response of the quantum anharmonic oscillator to the chirped parametric modulation involves successive transitions between neighboring *even* energy levels, i.e., the PLC. We define the anharmonicity parameter  $P_2 = 2\gamma/\sqrt{\alpha}$  [17, 18] ( $P_2 = 10$  in this example) and observe that the successive  $n \rightarrow n+2$  transitions

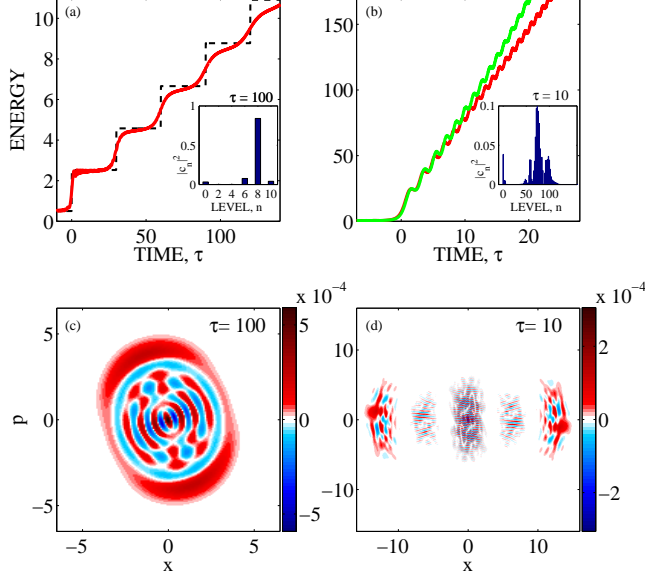


FIG. 1: (color online) The energy of the chirped parametric oscillator in the quantum PLC (a) and the classical PAR (b) regimes versus the slow time  $\tau$ . In (b), the Schrodinger simulation (red line) is compared to the classical solution (green line). The inserts are snapshots of the quantum state in the energy basis at given times. The corresponding snapshots of the Wigner distributions are shown in (c) and (d).

occur at times  $\tau_n = 4nP_2$ , in agreement with the theory below (dashed black line). To our knowledge, such ladder climbing dynamics in the parametrically modulated anharmonic oscillator is observed for the first time.

The second example (shown in Figs. 1(b,d)) uses the same initial conditions, but  $\{\alpha, \beta, \varepsilon\} = \{10^{-4}, 10^{-3}, 0.04\}$  and 250 levels. Here,  $P_2 = 0.075$  corresponding to the classical limit [17, 18], where the dynamics involves many energy levels and the energy grows as expected in the classical PAR [6, 10]. We compare this example with the classical simulations for the same Hamiltonian (1), i.e. solve

$$d^2x/dt^2 + (1 + \varepsilon \cos \varphi)x + \beta x^3 = 0 \quad (5)$$

with the same parameters. The unique characteristic of the classical parametric resonance is the existence of an unstable fixed point at zero energy [1]. Therefore, the chirped excitation in the classical case must involve nonzero initial conditions, e.g., a finite energy with random phases, as considered in Ref. [10], or a thermal distribution of initial conditions, i.e.,  $f(x_0, u_0) = (2\pi T)^{-1} \exp[-(x_0^2 + u_0^2)/(2T)]$ , where  $u = dx/dt$ . The latter choice is more suitable for studying the classical-quantum correspondence. We use  $T = 0.5$  associated with the energy of the quantum mechanical ground state of the unmodulated linearized system in these simulations. The classical averaged energy over 1000 realiza-

tions is plotted in green in Fig. 1(b) showing a good agreement with the quantum simulations. The deviation at large times is due to higher order corrections of the energy levels not included in Eqs. (3) and (4). The fact that the classical results can be reconstructed by solving the quantum equations implies that the correspondence principle is satisfied in the limit of small anharmonicity ( $\beta \ll 1$ ), where many energy levels are coupled simultaneously [17, 18].

For further illustration, we have calculated the phase-space Wigner distribution [23] in both examples above and show the snapshots at intermediated times in Fig. 1(c,d). In the first example (PLC), the Wigner distribution at  $\tau = 100$  exhibits structure characteristic to  $n = 8$  level of the quantum ladder, as expected from the energy levels occupation at the same time (see Fig. 1(a)). In the PAR example at  $\tau = 10$  in Fig. 1(d), the most populated parts of the phase space are two symmetrically separated resonantly trapped phase space regions of the parametric oscillator, while the characteristic interference patterns are seen in the nonresonant regions of phase space. The splitting of the trapped area in phase-space into two is explained as a pitchfork bifurcation [7].

*Quantum saturation.*— One of the important observables of the parametrically chirped oscillator is the probability of capture into resonance. One can define this probability quantum-mechanically as the total occupation of resonant levels after the sweeping of the modulation frequency through the linear resonance [17], or classically, as the fraction of the initial conditions leading to the phase-locked solution [24]. Thus, studying this probability comprises a good framework in discussing the quantum-classical correspondence in our problem (see a similar discussion in the direct AR and LC cases in Refs. [11] and [16, 19], respectively). In the direct AR scenario for a given temperature, the capture probability is a smoothed step function of the driving amplitude  $\varepsilon$  [24]. The threshold for capture into resonance in this case was defined as the value of the driving parameter  $\varepsilon_{\text{cr}}$ , yielding 50% capture probability, i.e.  $\varepsilon_{\text{cr}} = \varepsilon(P = 0.5)$ , while the transition width  $\Delta\varepsilon$  was the inverse slope of  $P(\varepsilon)$  at  $\varepsilon = \varepsilon_{\text{cr}}$ .  $\varepsilon_{\text{cr}}$  is temperature independent while  $\Delta\varepsilon$  scales as  $\sqrt{T}$  [17, 24]. Chirped Josephson circuit experiments revealed that at low temperatures, the AR threshold width saturates to a finite value, associated with the ground state of the unperturbed oscillator due to zero point quantum fluctuations [16, 17]. This quantum saturation effect was included in the classical AR theory by introducing an effective temperature  $T \rightarrow T_{\text{eff}} = \frac{\hbar\omega_0}{2k_B} \coth\left(\frac{\hbar\omega_0}{2k_B T}\right)$ , characterizing the thermal state in the Wigner phase-space representation [17]. In contrast to the direct AR, the low temperature behavior in the PAR has not been studied previously and is discussed next. Numerical simulations of Eqs. (4) show a typical S-shape dependence  $P(\varepsilon)$ , as in the insert of Fig. 2, which is similar to that in the direct AR [24]. Therefore, we define the threshold  $\varepsilon_{\text{cr}}$  for the PAR similarly, i.e.  $\varepsilon_{\text{cr}} = \varepsilon(P = 0.5)$ . In the theory

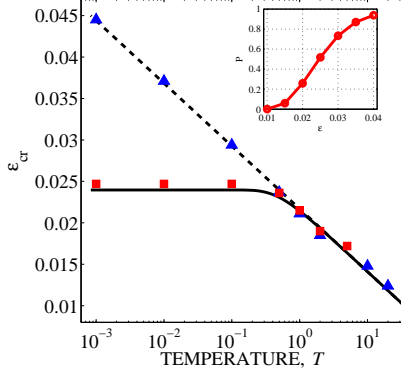


FIG. 2: (color online) The threshold on the modulation amplitude for resonant transition in the chirped parametric oscillator versus initial temperature: the classical simulations (blue  $\blacktriangle$ ), the theoretical scaling (6) (dashed line), the Schrodinger simulations (red  $\blacksquare$ ) exhibiting quantum saturation, and generalized theory (7) (solid line). The insert shows the capture probability  $P(\varepsilon)$  at  $T = 0.1$  in the quantum simulations (the threshold in this case is  $\varepsilon_{\text{cr}} = 0.0246$ ).

of the classical PAR [10],  $\varepsilon_{\text{cr}}$  was defined as  $\varepsilon(P = 0.1)$  due to the asymmetry of  $P(\varepsilon)$  for a fixed initial energy. Nonetheless, for a thermal distribution of initial conditions,  $P(\varepsilon)$  is symmetric, and  $\varepsilon(P = 0.5)$  is a preferable definition. A classical theory of the PAR was developed in [10], showing that the critical driving amplitude scales logarithmically with the initial action  $S_0$  of the oscillator,  $\varepsilon_{\text{cr}} \sim -\ln S_0$ . Therefore, we expect a similar scaling with the initial temperature,

$$\varepsilon_{\text{cr}}^{\text{PAR}}(T) = a - b \ln T. \quad (6)$$

We verify this scaling in numerical simulations of the classical equation of motion (5) subject to random, thermally distributed initial condition [25]. The results are shown in Fig. 2 (blue triangles) for  $\alpha = 0.0001$ ,  $\beta = 0.001$ . The logarithmic scaling is seen in the semi-log figure, while the best-fitted theoretical parameters in this case are  $a = 0.0217$  and  $b = 0.0033$ . Note that this classical scaling predicts an infinitely large driving amplitude for efficient capture into PAR in the limit of  $T \rightarrow 0$ . This singularity is removed if quantum fluctuations are taken into account. To illustrate this, we solve the Schrodinger equation (4) associated with Hamiltonian (1) using the parameters of the aforementioned classical simulations. The anharmonicity here is small,  $P_2 = 0.075 \ll 1$ , so many levels are simultaneously coupled at all times and the dynamics is classical, as illustrated in the insert of Fig. 1(b). The numerical quantum results for  $\varepsilon_{\text{cr}}(T)$  are presented by red squares in Fig. 2, showing a good agreement with the classical simulations for temperatures  $T > 0.5$ , but exhibit saturation of the threshold at low temperatures. This effect is similar to the quantum saturation of the transition width observed in the direct AR Josephson junction experiment [16]. To include this new effect in the theory, we replace  $T \rightarrow T_{\text{eff}} = \frac{1}{2} \coth\left(\frac{1}{T}\right)$  in

the classical expression for the threshold (6), i.e.

$$\varepsilon_{\text{cr}}^{\text{PAR}}(T) = a - b \ln T_{\text{eff}}. \quad (7)$$

This prediction with the coefficients  $a, b$  mentioned previously is shown by a solid line in Fig. 2 and agrees very well with the quantum numerical results at all temperatures. The replacement  $T \rightarrow T_{\text{eff}}$  can be explained via the Wigner phase-space representation. Indeed, the thermal state of the phase-space representation of a linearized oscillator is  $W(x_0, p_0) = (2\pi T_{\text{eff}})^{-1} \exp[-(x_0^2 + p_0^2)/(2T_{\text{eff}})]$ , while the quantum Liouville equation coincides with the classical Liouville equation in the limit  $P_2 \rightarrow 0$ . Thus, generally, quantum fluctuations in systems exhibiting classical dynamics, are taken into account by replacing  $T \rightarrow T_{\text{eff}}$  in the classical theory. Physically, the quantum uncertainty principle imposes a limit on the minimal area of the ground state (at  $T = 0$ ) in phase space, while classically, it becomes infinitesimally small. This imposes a quantum mechanical upper limit on  $\varepsilon_{\text{cr}}^{\text{PAR}}$ , corresponding to the quantum ground state at  $T \rightarrow 0$  ( $T_{\text{eff}} = 0.5$ ). This completes our discussion of the quantum saturation of the classical PAR at low temperatures. The second quantum limit, where only few levels are coupled simultaneously at all times and the dynamics becomes that of the PLC is discussed next.

*Classical-quantum correspondence.*— For studying the transition between the classical PAR and the quantum PLC regimes, we transform to the rotating frame as follows. First, we define  $C_n = c_n e^{iE_n t}$ , and rewrite Eq. (4) in the form

$$i \frac{dC_n}{dt} \approx \frac{\varepsilon}{8} (\sqrt{Q_{n+1}} C_{n+2} e^{-i(\omega_{n,n+2} t - \varphi)} + \sqrt{Q_{n-1}} C_{n-2} e^{i(\omega_{n-2,n} t - \varphi)}), \quad (8)$$

where  $\omega_{n,n+2} = E_{n+2} - E_n = 2 - \gamma(4n+6)$  and we neglect nonresonant terms (rotating wave approximation). Next, we introduce  $B_n = C_n \exp[-i \int \tilde{\Gamma}_n dt]$ , where  $\tilde{\Gamma}_n = \gamma Q_n - \frac{1}{2} n \alpha t$  and  $\tau = \sqrt{\alpha} t$ . Then, Eq. (8) can be written as

$$i \frac{dB_n}{d\tau} = \Gamma_n B_n + P_1 \left( \sqrt{Q_{n+1}} B_{n+2} + \sqrt{Q_{n-1}} B_{n-2} \right), \quad (9)$$

where  $\Gamma_n = \tilde{\Gamma}_n / \sqrt{\alpha} = \frac{n}{2} (P_2(n+1) - \tau)$  and  $P_1 = \frac{\varepsilon}{8\sqrt{\alpha}}$ ,  $P_2 = \frac{2\gamma}{\sqrt{\alpha}}$ . We have solved the slow Eqs. (9) numerically, subject to the ground state initial conditions,  $B_n(\tau_0 = -10) = \delta_{n,0}$ , and calculated the resonant capture probability  $P(P_1)$  for different values of the anharmonicity parameter  $P_2$ . The numerics of these slow equations is less time consuming, still yielding a good agreement with the solutions of the exact equations (8) (not shown). Similar to the definition of  $\varepsilon_{\text{cr}}$ , we define the threshold modulation parameter  $P_1^{\text{cr}} = P_1(P = 0.5)$  and show  $P_1^{\text{cr}}$  in Fig. 3 for different values of the anharmonicity  $P_2 \in [0.0035, 7.1]$  (green circles), covering both the classical PAR and the quantum PLC regimes. We also

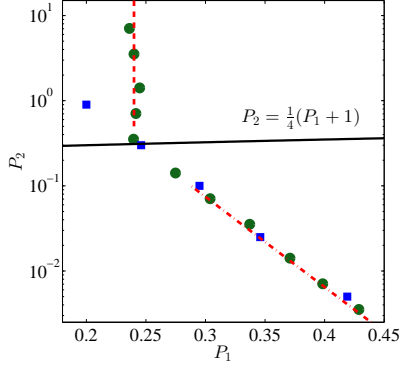


FIG. 3: (color online) The threshold,  $P_1^{\text{cr}}$  in  $(P_1, P_2)$  parameter space: Shrodinger simulations (green  $\bullet$ ), the PLC theory  $P_{1,\text{cr}}^{\text{PLC}} = 0.237$  (dashed red line), the PAR theory (13) (red dashed dotted line), and the classical simulations (blue  $\blacksquare$ ). Black solid line separates the classical PAR and the quantum PLC regimes.

calculate the corresponding classical threshold for different  $P_2$  by solving the classical equations (5) subject to the initial “ground state” temperature  $T = 0.5$ . The resulting  $P_{1,\text{class}}^{\text{cr}}(P_2)$  is shown in Fig. 3 (blue squares) and agrees well with the quantum calculations in the classical regime,  $P_2 \ll (P_1 + 1)/4$  (see below).

*The theory.*— Next, we develop a theory for  $P_1^{\text{cr}}(P_2)$  in both the quantum PLC and the classical PAR regimes. In the PLC regime, we assume a sufficiently large anharmonicity in the quantum PLC regime, such that only two levels are efficiently coupled as the modulation frequency passes the resonance  $\omega \approx \omega_{n,n+2}$ . In this case, the dynamics is that of successive  $n \rightarrow n + 2$  LZ transitions [20], where the avoided resonant crossing condition occurs when the diagonal terms of the two coupled levels are equal. Therefore, the time of the  $n^{\text{th}}$  parametric LZ transition is derived by equating the diagonal terms in Eq. (9), i.e.,  $\Gamma_n = \Gamma_{n+2}$ . By solving for  $\tau$ , one finds that the time of the  $n \rightarrow n + 2$  transition is  $\tau_n = 2nP_2$ . Therefore, the time interval between successive parametric LZ transitions in the PLC limit is  $\Delta\tau = \tau_{n+2} - \tau_n = 4P_2$ , in agreement with the example in Fig. 1(a) where  $P_2 = 10$ , so  $\Delta\tau = 40$ . Next, we write the reduced matrix of the  $n \rightarrow n + 2$  transition (see Eq. (9))

$$\begin{pmatrix} \frac{1}{2}P_2Q_n - \frac{1}{2}n\tau & P_1\sqrt{Q_{n+1}} \\ P_1\sqrt{Q_{n+1}} & \frac{1}{2}P_2Q_{n+2} - \frac{1}{2}(n+2)\tau \end{pmatrix}. \quad (10)$$

The typical time of the  $0 \rightarrow 2$  LZ transition in the adiabatic limit is  $\Delta\tau_{\text{LZ}} = P_1$  and unity in the nonadiabatic limit [24, 26]. Therefore, the theoretical condition for well separated successive LZ transitions (i.e., PLC),  $\Delta\tau \gg \Delta\tau_{\text{LZ}}$ , yields  $P_2 \gg \frac{1}{4}(P_1 + 1)$ . In this limit, the probability of each  $n \rightarrow n + 2$  transition is given by the LZ formula [20],

$$P_{n \rightarrow n+2} = 1 - e^{-2\pi P_1^2 Q_{n+1}} \quad (11)$$

and the total probability for capture into the PLC starting from the ground state is  $P_{\text{total}} = \prod_{n=0}^{\infty} P_{n \rightarrow n+2}$ . Solving  $P_{\text{total}} = 0.5$  for  $P_1$ , yields the threshold for capture into the PLC,  $P_{1,\text{cr}}^{\text{PLC}} = 0.237$ , where only two first terms in the product are needed for less than 1% accuracy. This theoretical prediction is shown in Fig. 3 by a dashed red line and agrees well with the numerical simulations in the quantum PLC regime. In addition, the theoretical separator  $P_2 = \frac{1}{4}(P_1 + 1)$  (black solid line) predicts correctly the location of the transition between the quantum PLC and the classical PAR regimes.

Finally, in the PAR regime we write  $x = a \cos \theta$ , define the slow phase-mismatch  $\phi = 2\theta - \varphi$  and the rescaled amplitude  $A = \sqrt{P_2}a$ , employ the single resonance approximation, and average Eq. (5) over the fast phase of the oscillator. This yields [6]

$$\frac{dA}{d\tau} = 2P_1 A \sin \phi; \quad \frac{d\phi}{d\tau} = A^2 - 2\tau + 4P_1 \cos \phi, \quad (12)$$

where, as before,  $P_1 = \frac{\varepsilon}{8\sqrt{\alpha}}$ ,  $P_2 = \frac{3\beta}{4\sqrt{\alpha}}$ ,  $\tau = \sqrt{\alpha}t$ , and the initial thermal distribution is  $f(A_0) = \sigma^{-2}A_0 \exp[-A_0^2/2\sigma^2]$ ,  $\sigma^2 = 0.5P_2T$ . Then, the generalized expression for the threshold becomes

$$P_{1,\text{cr}}^{\text{PAR}}(T) = \kappa_0 - \kappa_1 \ln(P_2 T_{\text{eff}}) \quad (13)$$

where  $\kappa_0 = 0.165$  and  $\kappa_1 = 0.41$ , are obtained by comparing Eqs. (7) and (13). The numerical results in Fig. 3 agree with this prediction for  $T_{\text{eff}} = 0.5$  (red dashed-dotted line) in the classical  $P_2 \gg \frac{1}{4}(P_1 + 1)$  regime.

In summary, we have studied the problem of passage through the parametric resonance in a quantum anharmonic oscillator and identified the quantum counterpart of the classical PAR, i.e., the quantum PLC. We have developed a theory of the PLC and the PAR for thermal initial conditions and found the threshold of capture into resonance in both regimes. We have also studied the transition from the PLC to the classical PAR and illustrated both the classical and the quantum resonant dynamics in phase-space by the Wigner distribution. In addition, we have identified the effect of quantum saturation of the threshold for parametrically resonant transition at small temperatures due to zero-point fluctuations. The saturation defines the maximum modulation amplitude needed for efficient PAR excitation. These results pave the way for using the PLC and the PAR as robust control tools in quantum electronic or optical systems in such applications as quantum communication and computing. It also seems interesting to extend the study of the PLC to quantum systems of many degrees of freedom, such as complex molecules and coupled qubits for controlling different interacting degrees of freedom. Supported by the Israel Science Foundation (Grant No. 451/10).

- 
- [1] L. D. Landau, *Mechanics*, 3rd ed. (Oxford, 1976).
  - [2] R. Di Leonardo et al., Phys. Rev. Lett. **99**, 010601 (2007).
  - [3] P. A. Braun, Theor. Math. Phys. **41**, 1060 (1979).
  - [4] M. I. Dykman, M. Marthaler, and V. Peano, Phys. Rev. A **83**, 052115 (2011).
  - [5] T.V. Gevorgyan and G.Yu. Kryuchkyan, J. Contemp. Phys. (Armenian Ac. Sci.) **48**, 107 (2013).
  - [6] E. Khain and B. Meerson, Phys. Rev. E **64**, 036619 (2001).
  - [7] O. M. Kiselev and S. G. Glebov, Nonlinear Dynamics **48**, 217 (2006).
  - [8] M. Assaf and B. Meerson, Phys. Rev. E **72**, 016310 (2005).
  - [9] O. Ben-David, M. Assaf, J. Fineberg, and B. Meerson, Phys. Rev. Lett. **96**, 154503 (2006).
  - [10] J. Fajans, E. Gilson, and L. Friedland, Phys. Rev. E **62**, 4131 (2000).
  - [11] G. B. Andresen *et al.* (ALPHA Collaboration), Phys. Rev. Lett. **106**, 025002 (2011).
  - [12] A. Barak, Y. Lamhot, L. Friedland, and M. Segev, Optics Express **18**, 17709 (2010).
  - [13] G. Manfredi and P.A. Hervieux, App. Phys. Lett. **91**, 061108 (2007).
  - [14] J.R. Danielson, T.R. Weber, and C.M. Surko, Phys. Plasmas **13**, 123502 (2006).
  - [15] O. Naaman, J. Aumentado, L. Friedland, J.S. Wurtele, and I. Siddiqi, Phys. Rev. Lett. **101**, 117005 (2008).
  - [16] K. W. Murch, R. Vijay, I. Barth, O. Naaman, J. Aumentado, L. Friedland, and I. Siddiqi, Nature Phys. **7**, 105 (2011).
  - [17] I. Barth, L. Friedland, O. Gat, and A. G. Shagalov, Phys. Rev. A **84**, 013837 (2011). (2012).
  - [18] G. Marcus, L. Friedland, and A. Zigler, Phys. Rev. A **69**, 013407 (2004).
  - [19] Y. Shalibo, Y. Rofo, I. Barth, L. Friedland, R. Bialczack, J. M. Martinis, and N. Katz, Phys. Rev. Lett. **108**, 037701 (2012).
  - [20] L.D. Landau, Phys. Z. Sowjetunion **2**, 46 (1932); C. Zener, Proc. R. Soc. London A **137**, 696 (1932).
  - [21] I. Barth and L. Friedland, Phys. Rev. A. **87**, 053420 (2013).
  - [22] L. Landau and E.M. Lifshitz, *Quantum Mechanics (Non-Relativistic Theory)*, 3rd ed. (Butterworth Heinemann, Oxford, 1977) p. 136.
  - [23] W.P. Schleich, *Quantum Optics in Phase Space*, (Wiley-VCH Verlag, Berlin, 2001), Chap. 3.3, p.75.
  - [24] I. Barth, L. Friedland, E. Sarid, and A.G. Shagalov, Phys. Rev. Lett. **103**, 155001 (2009).
  - [25] Similar to the direct AR, the coupling of the driven oscillator to a thermal environment can be modeled by a deterministic oscillator (with no external noise) but with thermally distributed initial conditions, provided sufficiently slow diffusive time as comparison to the sweeping time of driving frequency through the linear resonance [24].
  - [26] N.V. Vitanov and B.M. Garraway, Phys. Rev. A **53**, 4288 (1996).